(4)

Technical Report 1331
February 1990

Normal-Mode and Phase-Integral Methods for Determining Phase and Group Velocities in Simple Underwater Acoustic Ducts

M. A. Pedersen, D. F. Gordon,
F. Hosmer

NAVAL OCEAN SYSTEMS CENTER

San Diego, California 92152-5000

J. D. FONTANA, CAPT, USN
Commander

R. M. HILLYER
Technical Director

ADMINISTRATIVE INFORMATION

This report is the first in a series that deals with mode coupling and double ducts. The work reported upon in this series was sponsored by the Naval Ocean Systems Center Independent Research Program. M. A. Pedersen contributed as a private individual. Earlier work, on which this series is based, was jointly supported by the Office of Naval Research, Code 4250A, and the Chief of Naval Material Laboratory Participation Special Focus Program.

Released by
E. F. Rynne, Jr., Head
Acoustic Analysis Branch

Under authority of
T. F. Ball, Head
Acoustic Systems and
Technology Division

CONTENTS

INTRODUCTION

Underwater acoustic propagation in double ducts with associated mode coupling has potentially useful applications, but before this phenomenon can be properly evaluated, mode theory must be extended into unfamiliar territory. In an effort to analyze double-duct propagation, a new method of formulating mode properties has been developed, resulting in canonical eigenvalues. These eigenvalues are valid for classes of sound-speed profiles rather than for individual sound-speed profiles. The above analysis also makes frequent reference to the relationships between rays and modes.

Ray theory and mode theory interface in a number of ways, among which are the WKB (Wentzel, Kramers, and Brillouin) and phase-integral formulations for approximating eigenvalues. Also group velocities as determined for either rays or modes can be compared. These alternative points of view are often required in interpreting double-duct propagation and in developing, implementing, and checking the canonical eigenvalue technique.

This report is the introductory report of a series which describe the canonical eigenvalue technique, develop equations for mode and phase-integral formulations, determine group velocities, and apply these techniques to single acoustic ducts as well as double ducts. This introductory report has several goals:

1. To introduce the concept of canonical eigenvalues.
2. To make improvements in the ray-theory approach to the phase-integral method.
3. To compare double-duct eigenvalues with their single-duct counterparts.
4. To provide a general theoretical background for use in subsequent reports.

The overall goal of this series of reports is to develop improved techniques for the analysis of eigenvalues in double-duct propagation. The original effort, which prompted this series, was a study of the coupling characteristics of double ducts. Various stages of the early work were presented in a series of papers.[1–4] Three NOSC reports have also been published.[5–7] Although Ref. 5 on double ducts presents many numerical results of interest, the mathematical formulation is much too complicated for a theoretical analysis which could adequately explain the results. Reference 5 describes a five-layer duct, which involves an eigenvalue matrix of rank nine.

Some simple ducts with eigenvalue matrices of rank two and three were analyzed next in an endeavor to develop an improved theoretical approach which might eventually address double ducts. These are the unbounded refractive duct and the same duct with a surface boundary. This analysis did indeed develop the seed of a new theoretical approach, which we have chosen to name the canonical eigenvalue method. This development is one of the subjects of the present report.

Reference 6 extends this development of the canonical eigenvalue method to multilayer profiles and addresses the application of the method to the normalization of eigenfunctions. Reference 7 presents numerical results of the theory of Ref. 6 as applied to one-layer bounded-ducts.

This report first presents in Section 1 the general equations of mode theory and of the ray-theory application of the phase-integral method. The analysis goes beyond that necessary for simple ducts. For example, the mode-theory equations are used in Ref. 6 for multilayer profiles, and the phase-integral equations are used in the double-duct analysis of Ref. 5. The major analysis here is contained in Section 2, which compares normal-mode and phase-integral results for phase and group velocities for three types of simple ducts and introduces canonical eigenvalues. Section 3 illustrates how the mode solutions discussed in the previous section can be used in the analysis of the double-duct configuration of Ref. 5. Section 4 develops the concept of canonical eigenvalues as functions of two mathematical variables as a logical extension of the simple cases of Section 2. Section 5 presents a summary.

SECTION 1. GENERAL THEORY

SOUND-SPEED PROFILE

The sound speed in each layer of the profile is expressed as

$$[C_i/C(Z)]^2 = 1 - 2\gamma_i(Z - Z_i)/C_i \tag{1}$$

where C_i, Z_i, and γ_i are the sound speed, depth, and sound-speed gradient, respectively, at the top of layer i. The report will only deal with the case of continuous sound speeds at layer interfaces; i.e., the sound speed at the top of layer i and at the bottom of layer $i - 1$ is the same, with a value of C_i. A useful alternative expression is

$$[1/C(Z)]^2 = 1/C_i^2 - 2\gamma_i(Z - Z_i)/C_i^3 \tag{2}$$

From Eq. 1 we determine that

$$dC/dZ = C^3\,\gamma_i C_i^3 \tag{3}$$

thus, if γ_{i0} is the slope at the bottom of layer i

$$\gamma_{i0} = C_{i+1}^3\,\gamma_i/C_i^3 \tag{4}$$

Let the number of profile layers be I. In some cases layer I will be an unbounded half space. It is of interest to determine the limits of C as Z increases without bound. Consider first the case of γ_I positive. Here C increases monotonically from C_I to an infinite value at

$$Z = Z_I + C_I/2\gamma_I \tag{5}$$

For values of Z greater than this value, the sound speed turns pure imaginary. When γ_I is negative, C decreases monotonically from C_I and approaches zero asymptotically as Z goes to infinity.

In the special case of an unbounded refractive duct, we must consider the limit of C in layer 1 as Z goes to minus infinity. The counterpart of Eq. 5 is

$$Z = Z_2 + C_2/2\gamma_{10} \tag{6}$$

Here Z_2 is the axial depth, C_2 is the axial sound speed, and γ_{10} is the gradient at the bottom of layer 1. The subscript 2 in Eq. 6 on Z and C is consistent with evaluation at the bottom of layer 1.

NORMAL-MODE FORMULATION

In the treatment to follow, we assume that the density is constant. For the sound-speed profile of Eq. 1, the unnormalized depth function in layer i may be written as

$$F_i(Z) = D_i\, Ai(-\zeta_i) + E_i\, B_i(-\zeta_i) \tag{7}$$

Here D_i and E_i are coefficients which are independent of Z, Ai and Bi are the Airy functions, and ζ_i is given by

$$\zeta_i(Z) = [a_i^3/(Z - Z_i) + \omega^2/C_i^2 - \lambda_n^2]/a_i^2 \tag{8}$$

In Eq. 8

$$a_i^3 = -2\,\gamma_i\,\omega^2/C_i^3 \tag{9}$$

The quantity λ_n is known by several names, viz, the mode wave number, the mode eigenvalue, and the separation constant. The boundary conditions and the interface-matching conditions form a system of homogeneous linear equations in the coefficients D_i and E_i. The number of equations is equal to the number of D_i plus the number of E_i. This system of equations has a nontrivial solution (nonzero) if and only if the determinant of the coefficient matrix of the D_i and E_i is zero. This determinant set to zero is the eigenvalue equation. The λ_n are the values of mode wave number for which the determinant is zero.

Equation 8 may be expressed in terms of C rather than Z:

$$\zeta_i(C) = (\omega^2/C^2 - \lambda_n^2)/a_i^2 \tag{10}$$

Equation 10 follows from Eq. 2, 8, and 9.

The mode phase velocity is somewhat easier to interpret and analyze than the mode wave number. The mode phase velocity is given by

$$C_p = \omega/\lambda_n \tag{11}$$

With the use of Eq. 9 and 11, Eq. 10 may be expressed as

$$\zeta_i(C) = [1 - (C/C_p)^2]\,(C_i/C)^2\,|\gamma_i|^{-2/3}\,\pi^{2/3} f^{2/3} \tag{12}$$

The phase velocity depends on mode number, as do D_i, E_i, F_i, and ζ_i. One might then consider designating the mode number by the use of double subscripts on these quantities. This will not be done since it is too cumbersome and not particularly helpful. We will make it clear when it becomes important to distinguish results for various modes.

In setting up the interface and boundary conditions, it is necessary to evaluate $\zeta_i(Z)$ at the upper and lower interfaces of the layer. We define the value at the upper interface as $\zeta_{i1} \equiv \zeta_i(Z_i) = \zeta_i(C_i)$. Equation 12 becomes

$$\zeta_{i1} = [1 - (C_i/C_p)^2]\, \pi^{2/3} f^{2/3}\, |\gamma_i|^{-2/3} \tag{13}$$

Similarly, we define the value at the lower interface as

$$\zeta_{i0} \equiv \zeta_i(Z_{i+1}) = \zeta_i(C_{i+1})$$

With the use of Eq. 4, we find that Eq. 12 becomes

$$\zeta_{i0} = [1 - (C_{i+1}/C_p)^2]\, \pi^{2/3} f^{2/3}\, |\gamma_{i0}|^{-2/3} \tag{14}$$

The interface condition at interface $i + 1$ requires evaluations of ζ_{i0} and also of $\zeta_{i+1,1} \equiv \zeta_{i+1}(Z_{i+1}) = \zeta_{i+1}(C_{i+1})$. Here we find that Eq. 13 becomes

$$\zeta_{i+1,1} = [1 - (C_{i+1}/C_p)^2]\, \pi^{2/3} f^{2/3}\, |\gamma_{i+1}|^{-2\backslash 3} \tag{15}$$

We now introduce the gradient ratio as defined by

$$\rho_i = (-\gamma_{i0}/\gamma_{i+1})^{1/3} \tag{16}$$

It follows then that

$$\zeta_{i+1,1} = \rho_i^2\, \zeta_{i0} \tag{17}$$

We are now ready to deal with interface conditions. At layer interface $i + 1$ the continuity of pressure leads to

$$D_i\, Ai(-\zeta_{i0}) + E_i\, B_i(-\zeta_{i0})$$

$$-D_{i+1}\, Ai(-\rho_i^2\, \zeta_{i0}) - E_{i+1}\, Bi(-\rho_i^2\, \zeta_{i0}) = 0 \tag{18}$$

The continuity of dF/dZ leads to

$$D_i\, a_i\, Ai'(-\zeta_{i0}) + E_i\, a_i\, Bi'(-\zeta_{i0})$$

$$-D_{i+1}\, a_{i+1}\, Ai'(-\rho_i^2\, \zeta_{i0}) - E_{i+1}\, a_{i+1}\, Bi'(-\rho_i^2\, \zeta_{i0}) = 0 \tag{19}$$

From Eq. 4 and Eq. 9, we note that

$$a_i^3 = -2\gamma_{i0}\,\omega^2/C_{i+1}^3 \tag{20}$$

It follows that

$$a_{i+1}^3 = \gamma_{i+1}\,a_i^3/\gamma_{i0} = -\rho_i^{-3}\,a_i^3 \tag{21}$$

With the use of Eq. 19, Eq. 21 may be simplified to

$$D_i\,\rho_i\,Ai'(-\zeta_{i0}) + E_i\rho_i\,Bi'(-\zeta_{i0})$$

$$+ D_{i+1}\,Ai'(-\rho_i^2\zeta_{i0}) + E_{i+1}\,Bi'(-\rho_i^2\,\zeta_{i0}) = 0 \tag{22}$$

Consider now various boundary conditions. For a free surface

$$D_1\,Ai(-\zeta_{11}) + E_i\,Bi(-\zeta_{11}) = 0 \tag{23}$$

For a rigid bottom at interface $I + 1$

$$D_I\,Ai'(-\zeta_{I0}) + E_I\,Bi'(-\zeta_{I0}) = 0 \tag{24}$$

In Eq. 24, we have cancelled a common factor of a_I.

Consider cases where the last layer is an unbounded half space. In the case of a single layer profile with $\gamma_1 > 0$, Eq. 23 reduces to

$$Ai(-\zeta_{11}) = 0 \tag{25}$$

If we consider the surface to be rigid rather than free, the counterpart of Eq. 25 is

$$Ai'(-\zeta_{11}) = 0 \tag{26}$$

For the case where layer $I + 1$ is an unbounded half space with $\gamma_{I+1} > 0$, E_{I+1} is zero in Eq. 18 and 22.

The boundary conditions become more complicated when the gradient at the top of the last layer is negative. Here the solution in the last layer is given as

$$F_i(Z) = D_i\,h_2(\zeta_i) \tag{27}$$

where h_2 is the modified Hankel function of order one third and represents a down-going acoustic wave. The solution of Eq. 7 is still valid since h_2 can be expressed as a linear combination of Ai and Bi with complex coefficients. However, Eq. 27 is a clearer representation. The counterparts of Eq. 25 and 26 are

$$h_2(\zeta_{11}) = 0 \tag{28}$$

and

$$h_2'(\zeta_{11}) = 0 \tag{29}$$

These single-layer cases are of only passing interest here because the mode eigenvalues have large imaginary components and are severely damped.

Of somewhat more interest is where layer $I + 1$ is an unbounded half space. Here, for certain duct configurations as treated in Ref. 1 to 3 and Ref. 5, there are low-order modes for which the imaginary eigenvalue components can be small enough to be ignored. Here, $E_I + 1$ is zero in Eq. 18 and 22, Ai is replaced by h_2 in Eq. 18, and Ai' is replaced by h_2' in Eq. 22.

A further case of interest is the unbounded refractive duct, which consists of two unbounded half spaces. Here, both E_1 and E_2 of Eq. 7 are zero, Eq. 18 reduces to

$$D_1 Ai(-\zeta_{10}) - D_2 Ai(-\rho_1^2 \zeta_{10}) = 0 \tag{30}$$

and Eq. 22 reduces to

$$D_1 \rho_1 Ai'(-\zeta_{10}) - D_2 Ai'(-\rho_1^2 \zeta_{10}) = 0 \tag{31}$$

The group velocity is useful in the analysis of double-duct propagation. The group velocity of mode theory is given by

$$C_g = 1/(d\lambda/d\omega)\,|_{\lambda = \lambda_n} \tag{32}$$

An exact method for evaluating Eq. 32 for large eigenvalue matrices is presented in Ref. 8. The group velocity can be expressed in terms of the phase velocity with the use of Eq. 11 and 32 as

$$C_g = C_p/[1 - f(dC_p/df)/C_p] \tag{33}$$

PHASE-INTEGRAL METHOD

The implementation of the phase-integral method, used in this report is given by

$$2\pi f(\tilde{T} - \tilde{R}/C_m) = E_b + E_s + (n - 1)2\pi \tag{34}$$

Here, $\tilde{R}$ is the ray cycle range, $\tilde{T}$ is the associated travel time, and C_m is the ray parameter. The quantities E_b and E are phase shifts associated with the lower and upper boundary conditions. For reflection from a free boundary, E_s or $E_b = 0$. For reflection from a rigid boundary, E_s or $E_b = \pi$. If the ray forms in apex or nadir, rather than reflecting from a boundary, E_s or $E_b = \pi/2$. The value of C_m which satisfies Eq. 34 yields an approximation to the phase velocity of mode n.

A derivation of Eq. 34 is given in Ref. 9, in which Eq. 34 establishes a constructive interference of waves as described by rays. Reference 9 also cites earlier work on this ray-theory approach. In contrast, when one encounters the phase-integral method in

the literature, it is usually associated with the WKB method and is not associated with ray theory per se. Reference 10 provides a thorough treatment in which the WKB solution is an approximation to mode eigenfunctions; whereas the phase integral, the left side of Eq. 6.7.12 of Ref. 10, gives the equation for the poles of the WKB approximation, i.e., the eigenvalues. In further exposition, Ref. 10 relates the WKB approximation to rays and eventually in Eq. 7.9.14 expresses the phase integral in terms of the cycle range and cycle time. This example of Ref. 10 is identical to Eq. 34 for E_s and $E_b = \pi/2$.

A further source of confusion is that some authors are not careful to distinguish between the WKB and phase-integral method but use these terms indiscriminately. For example, Ref. 11 describes the overall approach as a phase-integral method, reserving the term WKB for one expression in the approach. In contrast, Ref. 12 on page 90 refers to the WKB error when addressing eigenvalues rather than eigenfunctions. The present article is concerned only with the ray-theory application of Eq. 34 for approximating eigenvalues. The authors have no interest in the WKB method for approximating eigenfunctions.

Equation 34 has been used for many years as a valuable adjunct and guide to mode theory. For example, Ref. 4 outlines a number of applications of this method, where the phase and group velocities of various ray theories can be tested by a comparison with mode theory. We have encountered various examples in which inexplicable normal-mode results could be simply explained by their ray-theory counterparts of the phase-integral method. An example is given in Ref. 13, with results published in more detail in Ref. 14.

Equation 34 may be written as

$$\tilde{T} - \tilde{R}/C_m = \mathrm{f}^{-1}P(n) \tag{35}$$

where

$$P(n) = n \tag{36}$$

for reflection from two free boundaries

$$P(n) = n - 1/4 \tag{37}$$

for reflection from one free boundary

$$P(n) = n - 1/2 \tag{38}$$

for no boundary reflections

$$P(n) = n - 3/4 \tag{39}$$

for reflection from one rigid boundary; and

$$P(n) = n - 1 \tag{40}$$

for reflection from two rigid boundaries.

We will not deal with Eq. 36 or 40 in this report. However, we digress to point out a significant result. As we reviewed this material for the final draft, we were puzzled as to the interpretation of Eq. 40 for $n = 1$. The day before, we had obtained some peculiar numerical results for the mode 1 canonical eigenvalues of a duct with two rigid boundaries. In a rare case of serendipity, these two apparent anomalies resolved each other. When $n = 1$, Eq. 35 has no solution. For if the right side is zero, then the group and phase velocity must be the same for all rays — an impossible situation. The proper interpretation of the result is that mode 1 does not exist for rays which reflect from both boundaries. The peculiar canonical eigenvalue curves for mode 1 terminated before entering the regime of phase velocities larger than the larger of the two sound speeds at the boundaries. These abbreviated curves for mode 1 correspond to the solutions of Eq. 39, whereas all the other modes have portions that correspond to Eq. 40 as well as Eq. 39.

We carried this one step further by noting that the solutions of Eq. 35 are the same for mode n for two free boundaries as they are for mode $n + 1$ for two rigid boundaries with the same sound-speed profile. We checked this result against the canonical eigenvalues for these two boundary conditions and found that these eigenvalues were indeed almost the same. This result, documented in Ref. 6, is another example of how the phase-integral approach of ray theory complements mode theory.

Our interest here is mainly in cases where Eq. 35 can be solved explicitly for C_m. However, in many cases this cannot be done. The appropriate treatment is to solve Eq. 35 by iteration using Newton's method. We express Eq. 35 as

$$F(C_m) = \tilde{T} - \tilde{R}/C_m - f^{-1} P(n) = 0 \tag{41}$$

Newton's method may be written as

$$C_{m,k+1} = C_{m,k} - F(C_{m,k})/(\partial F/\partial C_m)_k \tag{42}$$

where $C_{m,k}$ is the result of the kth iteration and $C_{m,k+1}$ is the result of the $k + 1$ iteration. From Eq. 58 of Ref. 15, we note that

$$(\partial F/\partial C_m)_k = \tilde{R}C_{m,k})/C^2_{m,k} \tag{43}$$

Thus, the roots of Eq. 41 are relatively easy to determine by a simple ray theory program which can evaluate $\tilde{R}$ and $\tilde{T}$.

The group velocity of ray theory is given by

$$C_g = \tilde{R}/\tilde{T} \tag{44}$$

We now examine the relationship between Eq. 44, evaluated at the C_m of Eq. 41, and the mode group velocity as given by Eq. 33. We first note that

$$dC_m/df = -(\partial F/\partial f)/(\partial F/\partial C_m) \tag{45}$$

where F is given by Eq. 41. If we assume that $\tilde{R}$, $\tilde{T}$, and $P(n)$ are independent of f, we obtain

$$\partial F/\partial f = P(n)/f^2 \tag{46}$$

With the use of Eq. 43, we obtain

$$dC_m/df = -P(n)C^2{}_m/\tilde{R}f^2 \tag{47}$$

Substituting Eq. 47 into Eq. 33 with $C_m = C_p$ leads to

$$C_g = C_m/[1 + P(n)C_m/\tilde{R}f] \tag{48}$$

We may solve Eq. 41 for $\tilde{T}/\tilde{R}$ to obtain

$$C_g^{-1} = \tilde{T}/\tilde{R} = C_m^{-1}[1 + P(n)C_m/\tilde{R}f] \tag{49}$$

Since Eq. 49 is the reciprocal of Eq. 48, we have demonstrated that Eq. 44 gives results for ray theory which are identical to those of Eq. 33 for mode theory.

Before the alert reader points out some counterexamples to this result, we note several important assumptions in obtaining this result. The first of these is that $C_m = C_p$, i.e., the phase-integral method must give the correct phase velocities of mode theory. As we shall demonstrate later, in certain cases the phase-integral approach can be modified so as to be completely congruent with the mode-theory result; i.e., $C_p = C_m$ for all frequencies. Hence, $dC_p/df = dC_m/df$, and Eq. 33 must give the same result when evaluated with C_p or C_m.

Another important assumption in obtaining Eq. 48 is that $\tilde{R}$, $\tilde{T}$, and $P(n)$ are independent of f. The modified ray theory of Ref. 16 and 17 examine cases where $\tilde{R}$, $\tilde{T}$, and the boundary phase shifts are functions of frequency. For these cases, Eq. 46 is no longer valid. One of the areas of further investigation is to determine the extent to which the results of modified ray theory and the phase-integral approach agree with the exact results of mode theory.

Equations 34 to 49 are valid approximations for any profile model. We now proceed to determine C_m for the profile of Eq. 1. The ray theory solutions for this model can be obtained from Ref. 18. They are expressed in terms of the parameter b_i, where

$$b_i = -2\gamma_i C_i^{-3} \tag{50}$$

Now b_i is a constant for a given layer, which is a distinct advantage from a ray theory standpoint. Equation 50 relates the sound speed at any depth in the layer and the gradient at that depth to the constant b_i. Thus, in some cases one must take care with the indices in the use of Eq. 50 to replace b_i, because at a common interface between layers there are two values of γ_i.

From Eq. 21 and 22 of Ref. 18, we may write

$$\tilde{T} - \tilde{R}/C_m = (4/3C_m^3)\,\Sigma(\tan^3\theta_{i+1} - \tan^3\theta_i)/b_i \qquad (51)$$

Here, b_i is the constant for layer i, and the summation extends over all layers from the surface or ray apex to the ray nadir. This summation is over one-half the ray cycle. Hence, the coefficient in front of the summation is twice that which appears in Eq. 22 of Ref. 18. Here

$$\tan\theta_i = (C_m^2 - C_i^2)^{1/2}/C_i \qquad (52)$$

Equation 51 is valid for any multilayered model of the form of Eq. 1. This report will deal with several simple cases of interest, where C_m can explicitly be solved in closed form.

SECTION 2. EXAMPLES OF SIMPLE DUCTS

This section deals with the mode and phase-integral solutions of ducts A to C of Fig. 1. Duct 4 of Fig. 1 is discussed in Section 4. All these ducts have horizontal asymptotes at the finite values of depth given by Eq. 5. The normal-mode and phase-integral solutions for ducts A and B and the symmetric form of duct C are well known. Our purpose in reviewing these ducts is to provide an introduction to the concept of canonical eigenvalues and to set the stage for the solutions to the asymmetric form of duct C and to more complicated profiles such as profile 4.

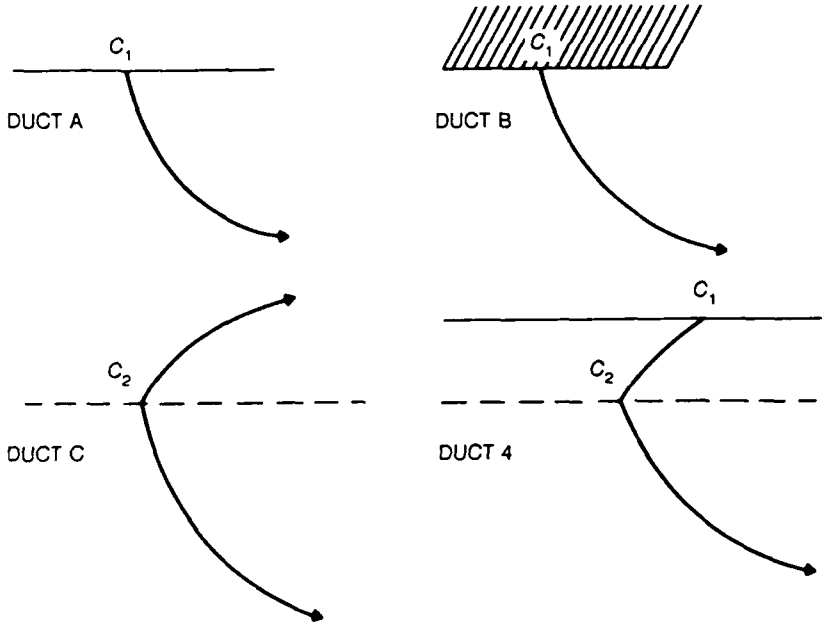

Figure 1. Schematic ducts of Sections 2 and 4, indicating boundaries and sound speeds in each layer. Layers are bounded by free or rigid surfaces, by layer interfaces, or by infinite values of sound speed.

FREE-BOUNDARY-SURFACE DUCT

Our concern here is a single-layer half space bounded above by a free surface, as illustrated by profile A in Fig. 1. The parameters of this duct are the surface sound speed C_1 and the surface gradient γ_1, which in most cases is restricted to be positive.

Mode-Theory Solution

In this case, ζ_{11} of Eq. 13 is the principal quantity in the solution. At this stage, we define a dimensionless mathematical variable, x, as

$$x \equiv \zeta_{11} \tag{53}$$

This may appear somewhat obtuse. The reason for the use of x is twofold. First, we simplify the notation. Second, we regard ζ_{11} as defined by the right side of Eq. 13; i.e., a function of the profile parameters, frequency, and phase velocity. On the other hand, we will regard x as the solution to a purely mathematical problem as defined by the eigenvalue equation. This is the concept of the canonical eigenvalue approach. The eigenvalue equation is solved in pure mathematical terms that include x and other mathematical variables. After the solution has been obtained in the mathematical variables, we transform the solution into the physical variables of interest. For example, if we know x, we may use Eq. 13 to obtain the phase velocity

$$C_p = C_1 \left[1 - f^{-2/3} \pi^{-2/3} \left|\gamma_1\right|^{2/3} x\right]^{-1/2} \tag{54}$$

Equations 53 and 54 will be applied to all canonical eigenvalue problems. We note that the absolute value signs in Eq. 54 are not necessary for our case of $\gamma_1 > 0$. However, Eq. 54 also applies to other problems where $\gamma_1 < 0$.

From Eq. 25, the solution for the single-layer surface duct with free surface is

$$Ai(-x) = 0 \tag{55}$$

The roots of Eq. 55 are the negative of the zeros of the Airy function as given in column 2 of Table III of Ref. 19. Column 2 of Table 1 presents the first ten zeros of Eq. 55, corresponding to the first ten normal modes.

The solid curves of Fig. 2 present the phase velocity of Eq. 54 for the first four roots (modes) of Table 1. The solid curves are nearly coincident, in this case, with the broken-line curves, which will be described later. For illustrative purposes, we have chosen C_1 = 1480 m/s and $\gamma_1 = 0.02\text{s}^{-1}$. From Eq. 54, it is evident that C_p approaches C_1 as a horizontal asymptote as the frequency is increased to infinity. The curves also form vertical asymptotes. These asymptotes are given by the zeros of the bracketed term in Eq. 54. They are

$$f = \left|\gamma_1\right| x^{3/2}/\pi \tag{56}$$

The phase velocity turns purely imaginary for frequencies less than that of Eq. 56.

Table 1. Zeros of $Ai(-x)$ and associated nonintegral mode number.

Zero Number j	Zero x_j	Asympt. Approx.	Modified n
1	2.3381	2.3204	1.00867
2	4.0879	4.0818	2.0395
3	5.5206	5.5172	3.00254
4	6.7876	6.7845	4.00187
5	7.9441	7.9425	5.00148
6	9.0227	9.0214	6.00122
7	10.0402	10.0391	7.00104
8	11.0085	11.0007	8.00091
9	11.9360	11.9353	9.00080
10	12.8288	12.8281	10.00072

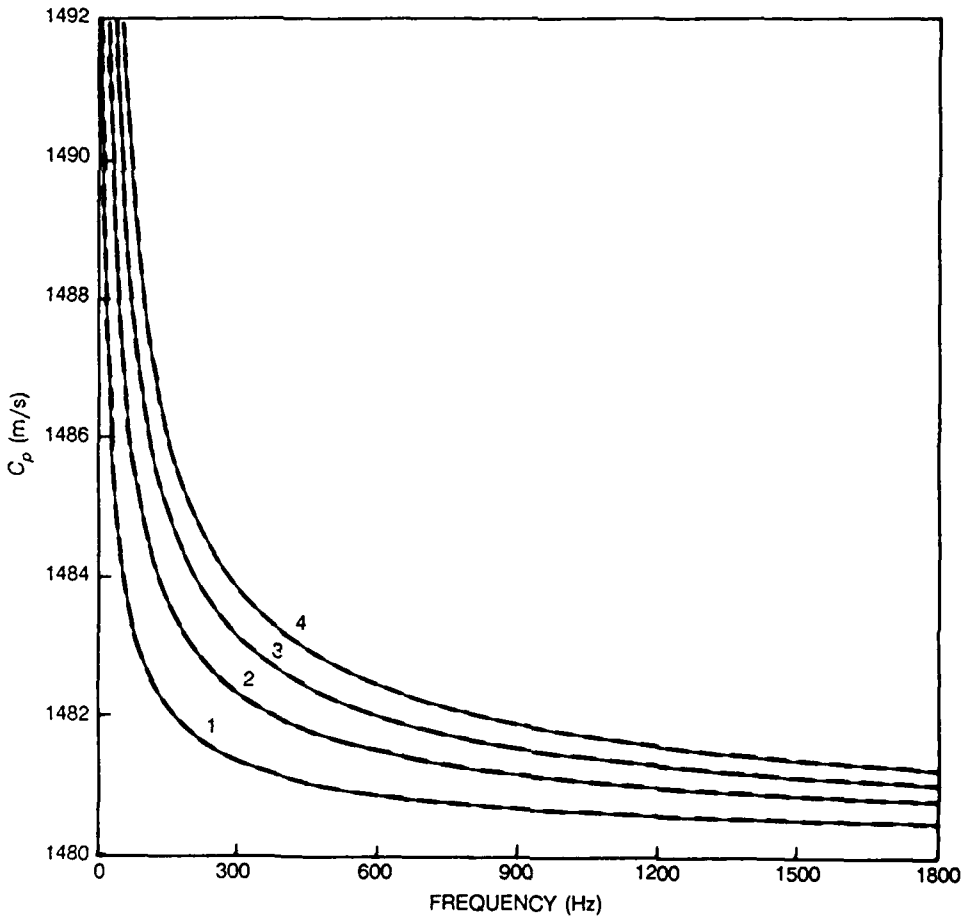

Figure 2. Phase velocity vs frequency for free-surface duct, compared for normal-mode (solid line) and phase-integral (dashed line) computation.

Since x is independent of frequency, it is relatively easy to obtain an expression for group velocity. Equation 33 may be evaluated from Eq. 54 and simplified to yield

$$C_g = C_p [1 + (C_p^2 - C_1^2)/3C_1^2]^{-1} \tag{57}$$

The solid curves of Fig. 3 present the results of Eq. 57. These curves were determined by evaluating Eq. 54 for a given frequency, evaluating Eq. 57 for this phase velocity, and plotting the result for the given frequency. From Eq. 57, it is apparent that as the frequency goes to infinity, C_g, as well as C_p, forms a horizontal asymptote at C_1. As C_p becomes infinite at the frequency of Eq. 56

$$C_g \rightarrow 0 \tag{58}$$

For values of frequency less than that of Eq. 56, C_g is purely imaginary.

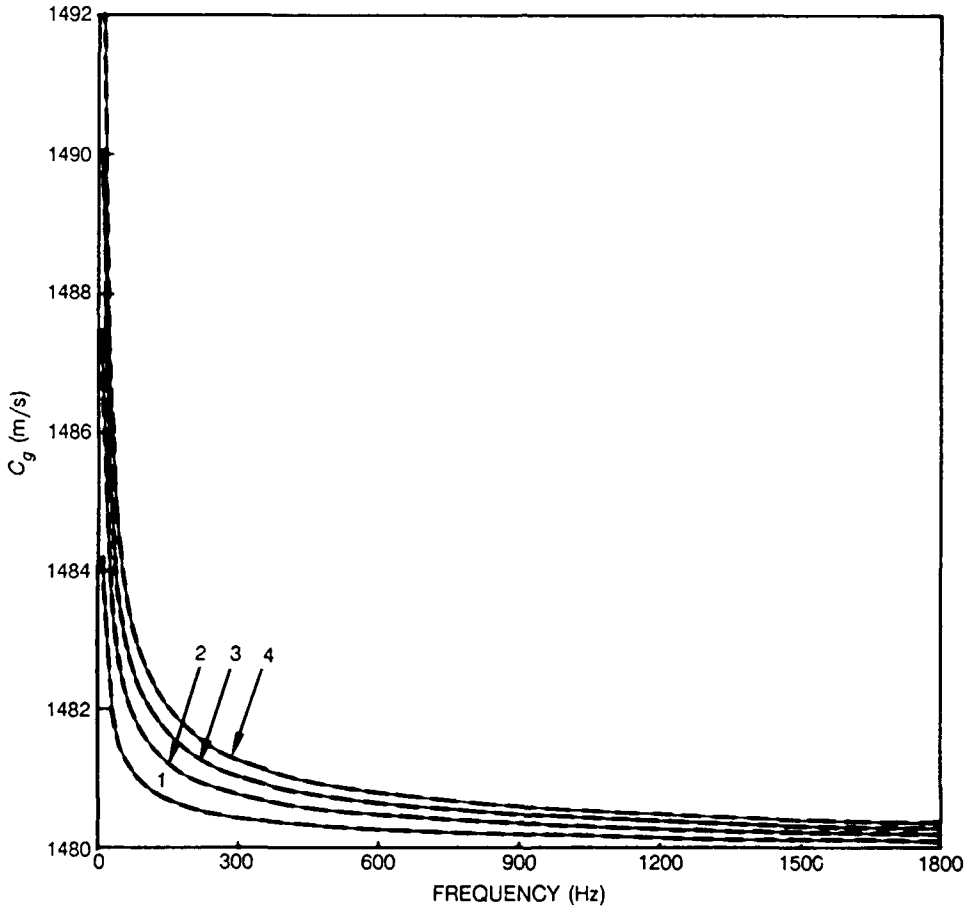

Figure 3. Group velocity vs frequency for free-surface duct, compared for normal-mode (solid line) and phase-integral (dashed line) computation.

One may differentiate Eq. 57 with respect to C_p and determine that C_g forms a relative maximum at

$$C_p = 2^{1/2} C_1 \tag{59}$$

The value of C_g at this point is

$$C_g = 3C_p / 4 \tag{60}$$

and the frequency is

$$f = |\gamma_1| \, x^{3/2} \, 2^{3/2} / \pi \tag{61}$$

Thus far we have considered $\gamma_1 > 0$. In the case of $\gamma_1 < 0$, Eq. 28 applies and the counterpart to Eq. 55 becomes

$$h_2(x) = 0 \tag{62}$$

The zeros of this modified Hankel function may be written as

$$x = -a_n \exp(2\pi i/3) \tag{63}$$

where the $-a_n$ are the roots of Eq. 55. In this case, the phase velocities of Eq. 54 are complex and, as discussed in Ref. 20, can be interpreted as the mode phase velocity and mode attenuation. We include this example to illustrate that the method of Eq. 54 can be applied to complex as well as real x.

Phase-Integral Solution

If we substitute Eq. 51 into Eq. 41 and solve for C_m, we obtain

$$C_m = C_1 [\, 1 - f^{-2/3} \, \gamma_1^{2/3} \, \pi^{-2/3} \, X]^{-1/2} \tag{64}$$

where

$$X = [3 \, P(n)/2]^{2/3} \, \pi^{2/3} \tag{65}$$

which for the case of Eq. 37 reduces to

$$X = [3(n - 1/4)/2]^{2/3} \pi^{2/3} \tag{66}$$

Here, we have included $\pi^{2/3}$ as a factor of X in order to make Eq. 64 resemble Eq. 54.

We next examine the relationship between x and X. The first term of the asymptotic expansion of $Ai(-x)$ may be written as[21]

$$Ai(-x) \sim \pi^{-1/2} \, x^{-1/4} \cos(\pi/4 - 2x^{3/2}/3) \tag{67}$$

The zeros then satisfy

$$\pi/4 - 2x^{3/2}/3 = n\pi \tag{68}$$

The solution of Eq. 68 is

$$x_n = \pi^{2/3}[3(n - 1/4)/2]^{2/3} \tag{69}$$

This is the same expression as Eq. 66. Thus, the phase-integral method gives phase velocities based on the zeros of the first term of the asymptotic expansion of $Ai(-x)$. This result comes as no surprise since the phase-integral approximation in general is often the same result as obtained by using the first term of the asymptotic expansion of the exact normal-mode solution.

The values of Eq. 69 are given in Column 3 of Table 1. A comparison with the exact zeros of Column 2 indicates a good approximation, which gets better with increasing root number, as should be expected for asymptotic expansions. The phase velocities based on Eq. 64 are shown in Fig. 2 as dashed curves, where they are almost indistinguishable from the solid curves derived from Eq. 54.

We can evaluate Eq. 44 for the group velocity, using Eq. 21 and 22 of Ref. 18. The result is Eq. 57, with C_p replaced by C_m. The dashed curves of Fig. 3 present the results of Eq. 57 evaluated at the phase velocity of Eq. 64 for the given frequency. Again the results are almost indistinguishable from the solid curves, obtained by evaluating Eq. 57 at the phase velocity of Eq. 54.

Equations 56 to 61 all hold for the phase-integral approach, with the x of mode theory replaced by the x_n of Eq. 69.

Reconciliation of Solutions

We note that the results of Eq. 54 and 64 agree when

$$x = X \tag{70}$$

We satisfy Eq. 70 by solving for n in Eq. 66. The solution is

$$n = (2\, x_j^{3/2}/3\pi) + 1/4 \tag{71}$$

where x_j is the jth root of Eq. 55. The values of Eq. 71 are given in Column 4 of Table 1. Thus, the phase-integral method can be made exact by the use of nonintegral values for mode number. We note also that the group velocity of ray theory, i.e., Eq. 44, also becomes exact because its equivalent, Eq 57, is evaluated at exact values of phase velocity.

Despite the sundry admonitions about the applicability of ray theory in the literature, we find in this case that the use of Eq. 71 leads to a ray-theory application which is completely congruent to the normal-mode results for phase and group velocity. The results are identical for all frequencies and can be applied to cases where the profile parameters C_1 or γ_1 are complex as well. The importance of nonintegral n is discussed in Section 4.

RIGID-BOUNDARY-SURFACE DUCT

The rigid-boundary-surface duct is illustrated by profile B of Fig. 1, where the free boundary of profile A, is replaced by a rigid boundary. The solutions are very similar to those of profile A, with Eq. 55 replaced by

$$Ai'(-x) = 0 \tag{72}$$

The roots of Eq. 72 are the negatives of the zeros of the Airy function derivative as given in Column 4 of Table III of Ref. 19. Column 2 of Table 2 presents the first ten zeros of Eq. 72.

Table 2. Zeros of $Ai'(-x)$ and associated nonintegral mode number.

Zero Number j	Zero x'_j	Asympt. Approx.	Modified n
1	1.0188	1.1155	0.96822
2	3.2482	3.2616	1.99229
3	4.8201	4.8263	2.99565
4	6.1633	6.1671	3.99697
5	7.3722	7.3749	4.99770
6	8.4885	8.4905	5.99814
7	9.5354	9.5371	6.99837
8	10.5277	10.5290	7.99868
9	11.4751	11.4762	8.99885
10	12.3848	12.3857	9.99894

The solid curves of Fig. 4 are obtained from Eq. 54 and are the counterparts of those of Fig. 2. Equation 56 gives the vertical asymptotes. The solid curves of Fig. 5 are obtained from Eq. 57, and Eq. 58 to 61, 64, and 65 hold. Equation 66 is replaced by

$$X = [3(n - 3/4)/2]^{2/3}\pi^{2/3} \tag{73}$$

The counterparts of Eq. 67 to 69 are

$$Ai'(-x) \sim \pi^{-1}x^{1/4} \cos(3\pi/4 - 2x^{2/3}/3) \tag{74}$$

$$3\pi/4 - 2x^{3/2}/3 = n\pi \tag{75}$$

and

$$x_n = \pi^{2/3}[3(n - 3/4)/2]^{2/3} \tag{76}$$

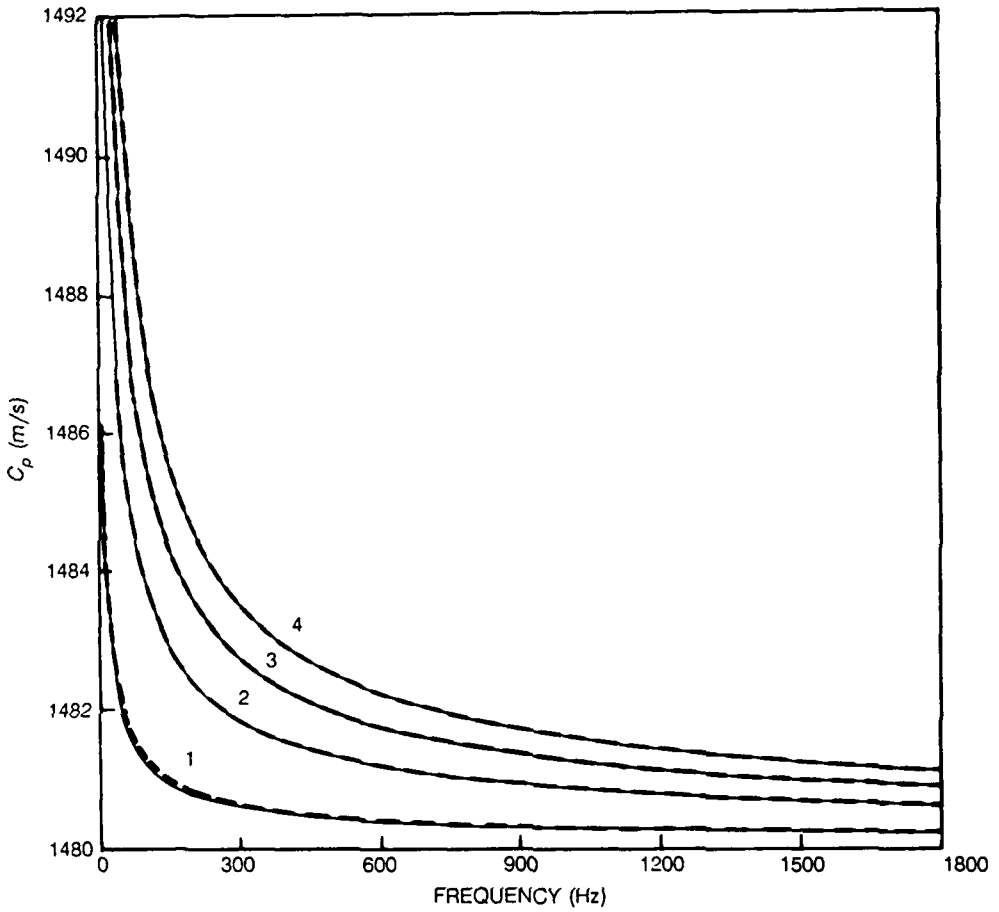

Figure 4. Phase velocity vs frequency for rigid-surface duct, compared for normal-mode (solid line) and phase-integral (dashed line) computation.

This is the same expression as Eq. 73. Thus, the phase-integral method gives phase velocities based on the zeros of the first term of the asymptotic expansion of $Ai'(-x)$.

The values of Eq. 76 are given in Column 3 of Table 2. The phase velocities based on Eq. 64 are shown in Fig. 4 as dashed curves. In contrast to Fig. 2, this asymptotic solution clearly differs from the solid curve based on Eq. 54.

The dashed curves of Fig. 5 are obtained from Eq. 57, using the phase velocities of Eq. 64. Equations 56 to 61 all hold for the phase-integral approach, with the x of mode theory replaced by the x_n of Eq. 76. The counterpart of Eq. 71 is

$$n = (2x_j'^{\,3/2}/3\pi) + 3/4 \tag{77}$$

where x_j' is the jth root of Eq. 72. The values of Eq. 77 are given in Column 4 of Table 2. Again, the phase and group velocities of ray theory are made exact by the use of nonintegral values for mode number.

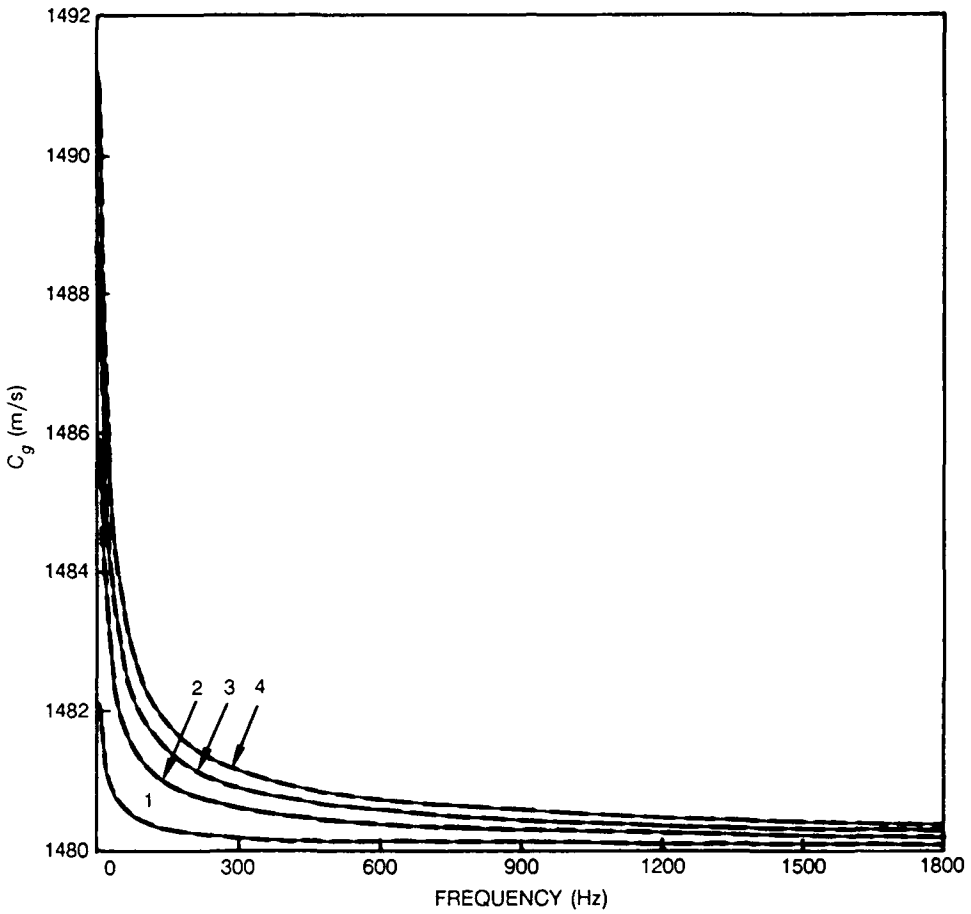

Figure 5. Group velocity vs frequency for rigid-surface duct compared for normal-mode (solid line) and phase-integral (dashed line) computation.

UNBOUNDED REFRACTIVE DUCT

The unbounded refractive duct is illustrated by profile C of Fig. 1. The axial sound speed is C_2, while the upper and lower gradients are γ_{10} and γ_2. This notation is consistent with the axis at the interface between layer 1 and layer 2.

Mode-Theory Solution

In this case, ζ_{10} of Eq. 10 is the principal quantity in the solution. We define another dimensionless variable, y, as

$$y \equiv \zeta_{10} \tag{78}$$

From Eq. 30 and 31, the canonical eigenvalue equation may be written as

$$G_1(y,\rho) = Ai(-y)\, Ai'(-\rho^2 y) + \rho Ai(-\rho^2 y)\, Ai'(-y) = 0 \tag{79}$$

In this report and in many applications, the only ρ_i of Eq. 16 is ρ_1. In Eq. 79 and hereafter, we will drop the subscript on ρ_1 to simplify the notation. Our use of the variable y will become apparent, when we deal with canonical eigenvalues of profile 4 in Section 4.

If we know y, we may use Eq. 13 to obtain the phase velocity

$$C_p = C_2 [1 - f^{-2/3}\pi^{-2/3} |\gamma_2|^{2/3}\rho^2 y]^{-1/2} \tag{80}$$

Alternatively, we may use Eq. 16 and 80 to obtain

$$C_p = C_2 [1 - f^{-2/3}\pi^{-2/3} |\gamma_{10}|^{2/3} y]^{-1/2} \tag{81}$$

Consider now the case of the symmetric duct, i.e., $\rho = 1$. Here, Eq. 79 reduces to

$$G_1(y,1) = 2Ai(-y)\, Ai'](-y) = 0 \tag{82}$$

Thus, the roots of Eq. 79 are given by those of Eq. 55 for even modes and by those of Eq. 72 for odd modes.

A computer routine was developed to solve Eq. 79 by Newton's method. The procedure starts at $\rho = 1$ with a known zero of $Ai(-y)$ or $Ai'(-y)$. The value of ρ is decreased by successive steps of $\Delta\rho$, and the solution of Eq. 79 is obtained for each step by the iteration

$$y_{i+1} = y_i + G_1(y_i,\rho)/(\partial G_1/\partial y)\,|_{y_i} \tag{83}$$

where

$$(\partial G_1/\partial y)\,|_{y_i} = -(\rho^3+1)[Ai'(-y_i)\, Ai'(-\rho^2 y_i) - y_i\, Ai(-y_i)\, Ai(-\rho^2 y_i)] \tag{84}$$

The initial estimate of y_i is taken to be the solution of Eq. 79 for the previous values of ρ. Once the iteration of Eq. 83 reaches the desired accuracy, the process is stopped, ρ is decreased by $\Delta\rho$, and the iteration process is repeated.

We note that the solution of Eq. 79 for $0 < \rho < 1$ suffices for all ρ. The solution y of Eq. 79 for ρ^{-1} is related to the solution $\bar{y}$ of Eq. 79 for ρ by

$$\bar{y} = \rho^{-2} y \tag{85}$$

Thus, if $\rho > 1$, we take the solution y for ρ^{-1} and then use Eq. 85 to determine $\bar{y}$, the solution for ρ.

When $\rho = 0$, Eq. 79 reduces to

$$G_1(y,0) = Ai(-y)\, Ai'(0) = 0 \tag{86}$$

Thus, the solutions for $\rho = 0$ are given by Eq. 55.

Figure 6 presents the solutions of Eq. 79 as a function of ρ for the four smallest roots, i.e., the first four modes. The horizontal lines are the zeros of $Ai(-y)$. They serve a double duty. This is the solution for all modes at $\rho = 0$ and for the even modes at $\rho = 1$. The solution for odd modes at $\rho = 1$ are the zeros of $Ai'(-y)$. Columns 2 and 4

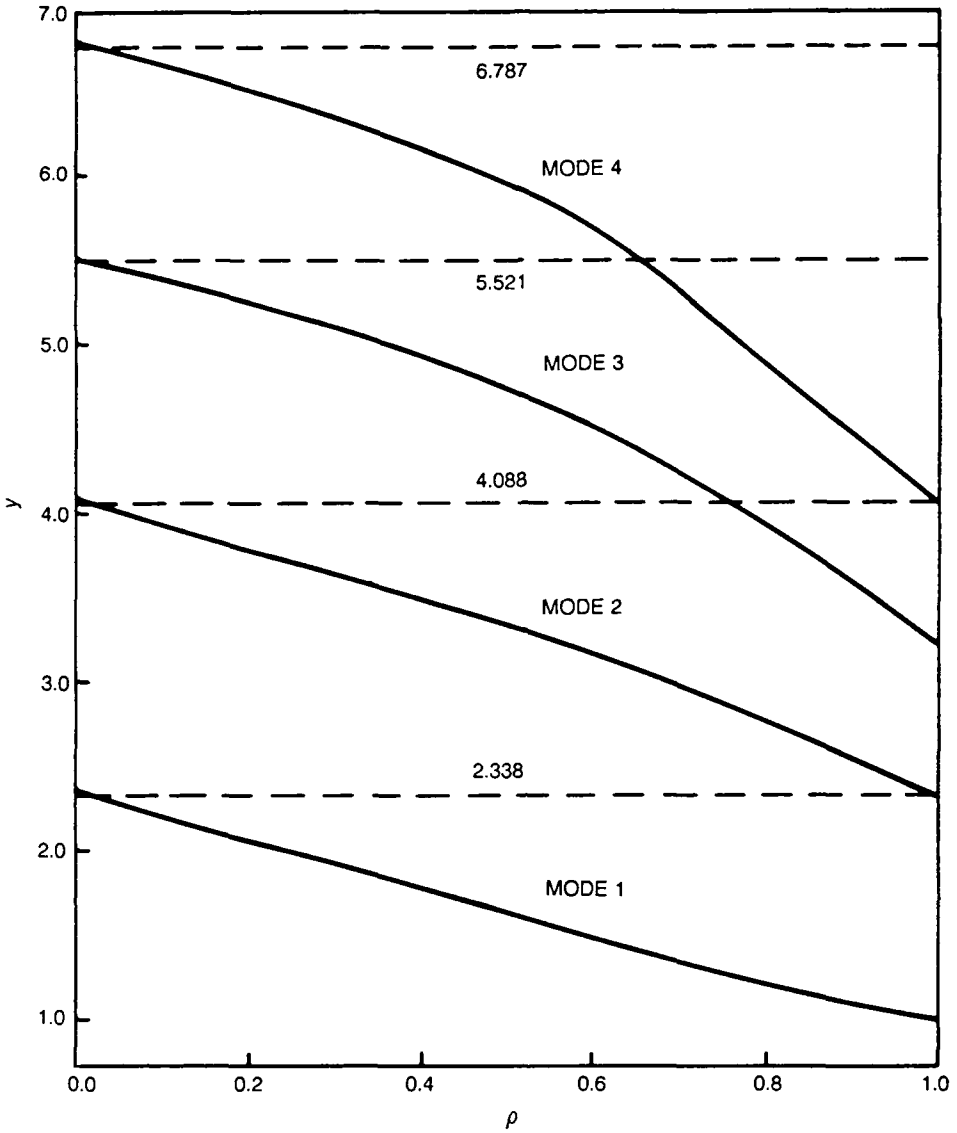

Figure 6. The canonical eigenvalues, y vs ρ, or the first four modes of the unbounded refractive duct. Here, ρ is the cube root of the negative of the ratio of axial gradients.

of Table 3 give the solutions of modes 1 and 2, respectively, for values of ρ at 0.05 increments from $\rho = 1$ to 0. The plots of Fig. 6 indicate that the solutions are extremely well-behaved functions of ρ. Thus, linear or higher order interpolation could be used to obtain very accurate values for arbitrary ρ from tabular values such as those of Table 3.

Table 3. Eignevalues y, for the first two modes of an unbounded refractive duct and associated nonintegral mode number.

	Mode 1		Mode 2	
ρ	Root y	Modified n	Root y	Modified n
1.00	1.01879	0.93643	2.33811	2.01734
0.95	1.07100	0.93685	2.45472	2.01587
0.90	1.12574	0.93824	2.56867	2.01048
0.85	1.18295	0.94070	2.68156	2.00410
0.80	1.24254	0.94440	2.78946	1.99483
0.75	1.30436	0.94949	2.89295	1.98468
0.70	1.36823	0.95611	2.99201	1.97496
0.65	1.43393	0.96444	3.08688	1.96697
0.60	1.50120	0.97462	3.17792	1.96186
0.55	1.56975	0.98679	3.26554	1.96059
0.50	1.63928	1.00106	3.35012	1.96387
0.45	1.70949	1.01753	3.43199	1.97215
0.40	1.78009	1.03625	3.51143	1.98568
0.35	1.85083	1.05724	3.58870	2.00451
0.30	1.92148	1.08047	3.66402	2.02850
0.25	1.99187	1.10603	3.73761	2.05734
0.20	2.06189	1.13331	3.80968	2.09057
0.15	2.13148	1.16259	3.88048	2.12761
0.10	2.20066	1.19346	3.95025	2.16775
0.05	2.26948	1.22561	4.01930	2.21017
0.00	2.33811	1.25868	4.08795	2.25395

There are two distinct physical configurations which correspond to $\rho = 0$. The first is $\gamma_{10} = 0$, which arises from an isospeed half space above the axis. The second is $\gamma_2 = \infty$, which arises from the limit of a steep positive gradient below the axis. Although the mathematical eigenvalues are the same for both configurations, the physical results are quite different. For $\gamma_{10} = 0$, the phase velocity of Eq. 81 reduces to C_2, the axial sound speed. For $\gamma_2 = \infty$, Eq. 81 depends in the usual manner on C_2, f, γ_{10}, and the zeros of $Ai(-y)$.

It is not convenient at this point to present a numerical example of phase velocity vs frequency as was done in Fig. 2 and 4. All numerical examples will be deferred to Section 3. Equations 56 to 61 hold, with γ_1, x, and C_1 replaced by γ_{10}, y, and C_2, respectively.

Phase-Integral Solution

For this profile, the phase-integral counterpart of Eq. 64 may be written as

$$C_m = C_2 [1 - f^{-2/3} \gamma_{10}^{2/3} \pi^{-2/3} Y]^{-1/2} \tag{87}$$

where

$$Y = [3P(n)/2]^{2/3} \pi^{2/3}(1 - \gamma_{10}/\gamma_2)^{-2/3} \tag{88}$$

From Eq. 38 and 16, this may be expressed as

$$Y = [3(n - 1/2)/2]^{2/3} \pi^{2/3}(1 + \rho^3)^{-2/3} \tag{89}$$

Equations 56 to 61 hold, with γ_1, x, C_p, and C_1 replaced by γ_{10}, Y, C_m, and C_2, respectively.

Some of the properties for the group velocities of ray and mode theory can be associated with the analysis of Ref. 22 for general classes of refractive ducts. From Eq. 80 of Ref. 22

$$L(C_g) = C_a \tag{90}$$

where L is the limit as C_m or $C_p \rightarrow C_a$, and C_a is the axial sound speed. As $f \rightarrow \infty$, C_m in Eq. 87 or C_p in Eq. 80 $\rightarrow C_2$, and C_g of Eq. 57 approaches $C_a = C_2$. Thus, Eq. 90 is satisfied.

Profile class C of Fig. 1 falls under the class of Ref. 22 for which the slopes at the axis are finite but not zero. For this class, Eq. 90 of Ref. 22 applies and is

$$L(dC_g/C_m) = 1/3 \tag{91}$$

If we differentiate the C_2 counterpart of Eq. 57 with respect to C_p, we obtain

$$dC_g/dC_p = C_g/C_p - 2C_p^2/3C_2^2 \tag{92}$$

The limit of this as $f \rightarrow \infty$ and C_p and $C_g \rightarrow C_2$ is

$$dC_g/dC_p = 1 - 2/3 = 1/3 \tag{93}$$

Thus, Eq. 91 is satisfied.

We can also explain the result of Eq. 58 as the phase velocity goes to infinity. Section III B.2.f. of Ref. 23 discusses how ray theory range varies as the phase velocity goes to infinity. It demonstrates that the range is infinite if there is no horizontal asymptote for the sound-speed profile. It is constant if there is a horizontal asymptote at infinite depth, and is zero if there is a horizontal asymptote at finite depth. Thus, $\tilde{R}$ for our profile is zero in the limit because of the horizontal asymptotes of Eq. 5 and 6.

Since $\tilde{T}$ is not zero for this limit, the group velocity goes to zero. Thus, the result of Eq. 58 is associated with the horizontal asymptotes of the sound-speed profile model.

We next examine the relationship between Eq. 87 and Eq. 80. For this purpose, we express Eq. 87 as

$$C_m = C_2[1 - f^{-2/3}H^{2/3}\pi^{-2/3}\,\overline{Y}]^{-1/2} \tag{94}$$

where

$$H = [(\gamma_2^{-1} + |\gamma_{10}|^{-1})/2]^{-1} \tag{95}$$

and

$$\overline{Y} = [3(n - 1/2)/4]^{2/3}\pi^{2/3} \tag{96}$$

Equations 94 and 96 are equivalent to Eq. 87 and 89 and are obtained by algebraic manipulation. The quantity H of Eq. 95 is the harmonic mean of the gradients.

We now consider a symmetric duct with gradients γ_{10} and $-\gamma_{10}$. The solutions for a symmetric duct are given by Eq. 82. Consider first the even modes. Here, Eq. 69 applies with

$$y_j = \pi^{2/3}[3(j - 1/4)/2]^{2/3} \tag{97}$$

Here, j is the root number which equals $n/2$. Equation 97 may be written as

$$y_{n/2} = \pi^{2/3}[3(2n - 1/2)/4]^{2/3} \tag{98}$$

Thus, for even modes, Eq. 98 is the same as Eq. 96.

Consider next the odd modes. Here, Eq. 76 applies with

$$y_j = \pi^{2/3}[3(j - 3/4)/2]^{2/3} \tag{99}$$

Here, j, the root number, equals $(n + 1)/2$ for odd modes. Equation 99 may be written as

$$y_{(n+1)/2} = \pi^{2/3}[3(n - 1/2)/4]^{2/3} \tag{100}$$

Thus, for odd modes, Eq. 100 is the same as Eq. 96.

For the refractive duct C of Fig. 1, the phase-integral method corresponds to the use of the first term in the asymptotic expansion of $Ai(-y)$ and $Ai'(-y)$ for a symmetric duct with a slope which is the harmonic mean of the absolute values of the axial slope. Note that this is an interpretation of the method; it implies nothing as to the accuracy of the method.

Reconciliation of Solutions

If we equate Eq. 89 to Eq. 81 and solve for n, we obtain

$$n = 2y^{3/2}(1 + \rho^3)/3\pi + 1/2 \tag{101}$$

Where y is the nth root of Eq. 79. In the special case of a symmetric duct, Eq. 101 can be expressed in closed form. In the case of even modes, Eq. 101 reduces to

$$n = 4\, x_j^{3/2}/3\pi + 1/2 \tag{102}$$

We note that Eq. 102 is just twice the result of Eq. 71 for the free-boundary-surface duct. In the case of odd modes, Eq. 101 reduces to

$$n = 4\, x'^{3/2}_j/3\pi + 1/2 \tag{103}$$

This result is twice the result of Eq. 77 minus 1.

The results of Eq. 103 for odd modes are given in Column 2 of Table 4. The results of Eq. 102 for even modes are given in Column 4. With the exception of mode 1, the modified values of n are not significantly different from integral values.

Table 4. Nonintegral mode numbers for a symmetric unbounded refractive duct.

Odd Mode Number	Modified n	Even Mode Number	Modified n
1	0.93643	2	2.01734
3	2.98458	4	4.00790
5	4.99131	6	6.00508
7	6.99396	8	8.00374
9	8.99537	10	10.00296
11	10.99625	12	12.00244
13	12.99685	14	14.00208
15	14.99729	16	16.00182
17	16.99761	18	18.00160
19	18.99787	20	20.00144

Columns 3 and 5 of Table 3 give the results of Eq. 101 for modes 1 and 2, respectively. In the case of mode 1, the value of modified n increases monotonically from 0.93643 for $\rho = 1$ to 1.25868 for $\rho = 0$. The phase integral approximation for the asymmetric duct for ρ greater than about 0.33 is no more inaccurate than it is for $\rho = 1$.

In the case of mode 2, the modified n decreases from 2.01734 for $\rho = 1$ and forms a minimum of about 1.960 at about $\rho = 0.55$. It then increases monotonically to

2.25395 for $\rho = 0$. Here, the difference between integral and nonintegral values is less than ±0.04 for ρ greater than about 0.33.

We conclude then that the phase-integral method is a reasonably good approximation to the asymmetric duct. For mode 1, the difference between modified and integral n is less than 0.064 for values of ρ greater than 0.33. The largest difference is 0.259, occurring at $\rho = 0$. For mode 2, the differences are less than ±0.039 for values of ρ greater than 0.33. The largest difference is 0.254, occurring at $\rho = 0$.

We are indebted to a JASA reviewer for calling our attention to Ref. 12 in which Tolstoy and Clay analyze the symmetric refractive duct. They assess the accuracy of the phase-integral approximation (referred to by them as the WKB or Bohr-Sommerfeld equation) by comparing it with the exact normal-mode solution. They also demonstrate that the phase-integral approximation corresponds to the use of the first term of the asymptotic expansion of the exact normal-mode solution. The Ref. 12 analysis is couched in terms of the customary WKB approach without regard for ray theory and illustrates a reviewer's observation that the phase-integral approximations of all the examples of Section 2 could be obtained without computing a single ray. This is indeed true, because in these examples, Eq. 34 can be solved for phase velocity in closed form. The importance of the discussion of the phase-integral method in Section 1 for more complicated profiles is presented at the end of Section 4.

SECTION 3. APPLICATION TO DOUBLE DUCTS

This section applies the results of Section 2 for the unbounded refractive duct to the double-duct profile of Ref. 1 to 3 and 5. It also illustrates how the canonical eigenvalues of Fig. 6 are translated to phase velocity vs frequency plots for two specific refractive ducts.

Figure 7, taken from Ref. 5, presents the double-duct sound-speed profile. It consists of an upper refractive duct bounded above by the surface and overlying a lower refractive duct. The lower refractive duct is bounded below by a negative-gradient half space.

Figure 8, taken from Ref. 5, presents phase velocity vs frequency for the profile of Fig. 7. The circles represent the mode 2 and 3 solutions for the double-duct profile as obtained by evaluating the eigenvalues at intervals of 0.5 Hz. The dashed curve is the phase-integral result of Eq. 87 and 89, evaluated for mode 1 of the upper duct. The solid curve is the phase-integral result evaluated for mode 2 of the lower duct. Observe that the difference between the phase velocities of mode 3 and mode 2 forms a minimum at about 53 Hz. We refer to this condition as a critical frequency because at the critical frequencies the coupling between the upper and lower ducts is strong. Now the critical frequencies are approximated by the intersections of the phase-integral curves for the two individual ducts. In this case, the intersection labeled crossing B at about 60 Hz is the approximation to the critical frequency at about 53 Hz.

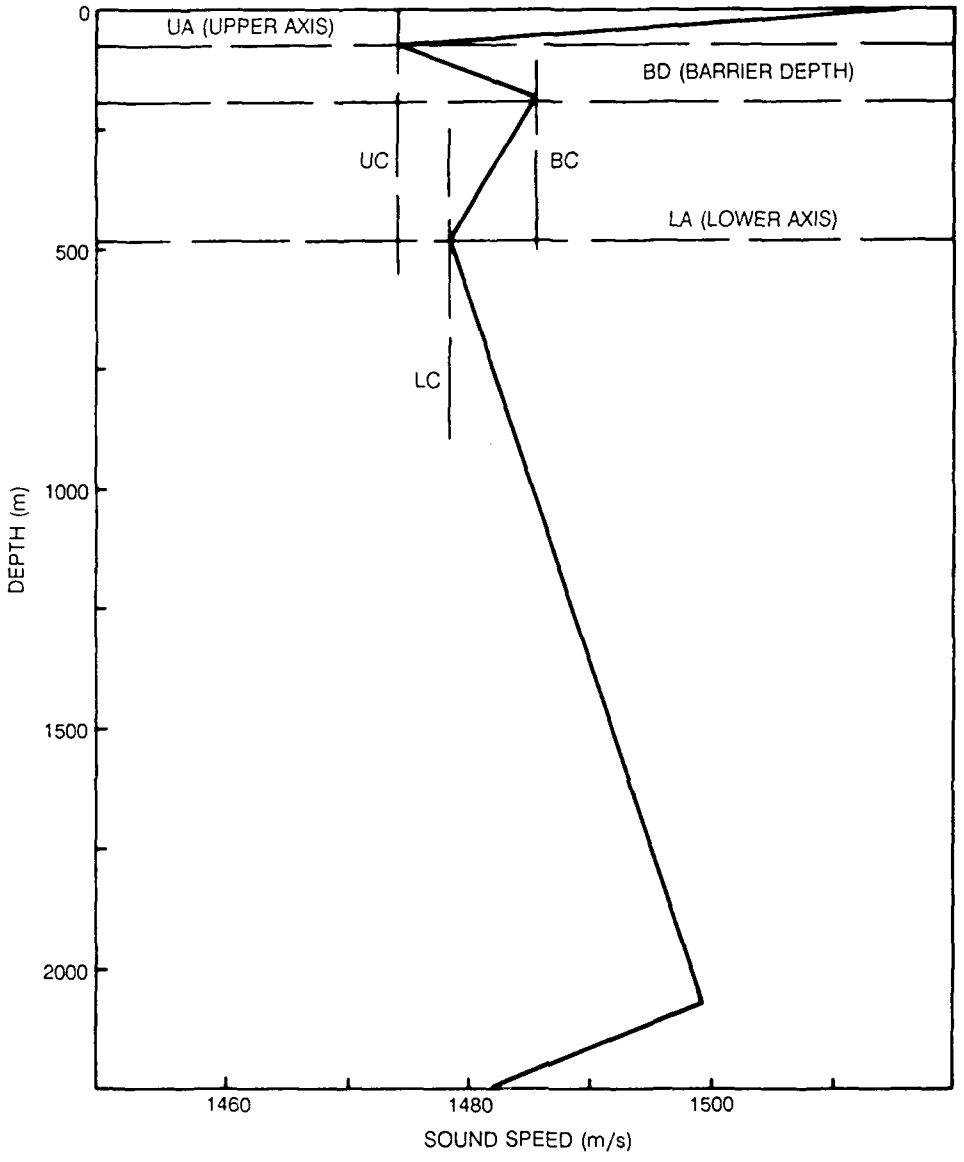

Figure 7. The double-duct sound-speed profile used in the analysis of Ref. 5.

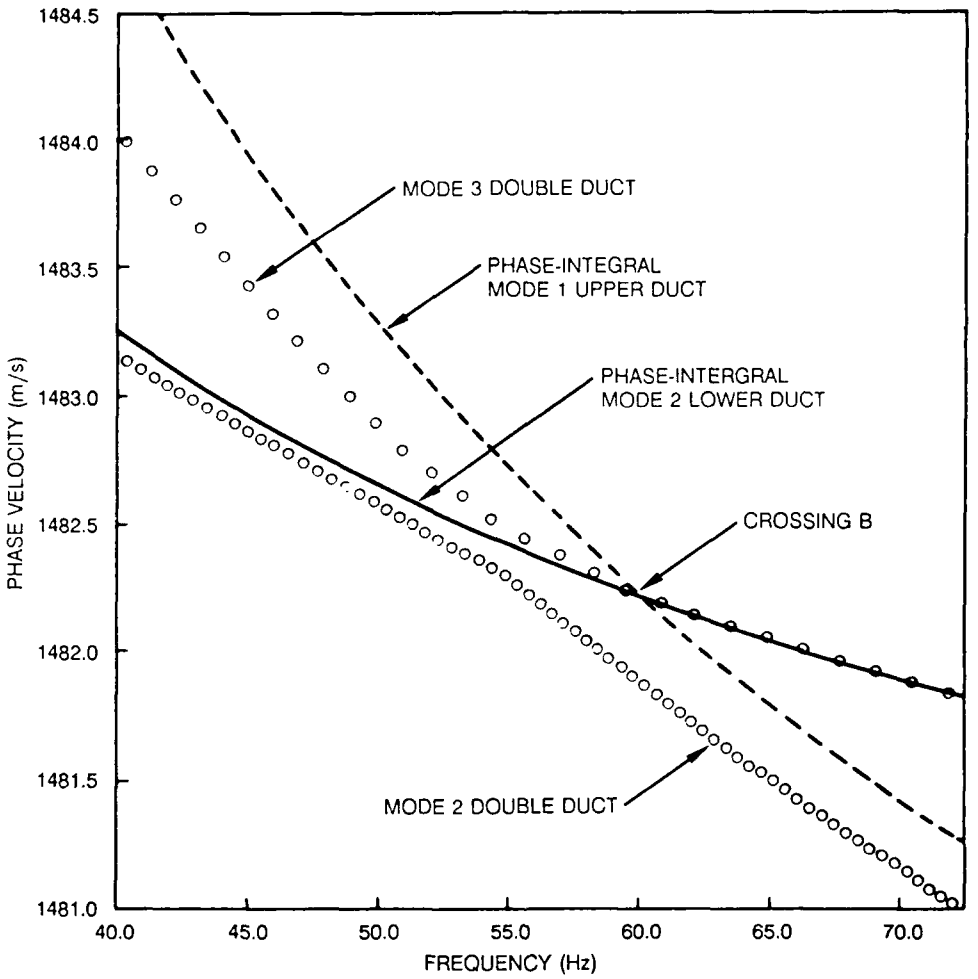

Figure 8. Phase velocity vs frequency for a double duct compared to phase-integral results for the two single ducts.

When Fig. 8 was first generated some five years ago, we became interested in developing a method to improve the accuracy of the phase-integral method. It is important to obtain an accurate estimate, because the evaluation of double ducts by mode theory is a much more laborious process than to apply the phase-integral method to help zero in on the critical frequency regions.

The first step in this investigation was to compare the normal-mode results for the single unbounded ducts with the phase-integral results. Figure 9 gives the results for modes 1 to 4 of the lower duct and for modes 1 and 2 of the upper duct. Again, the curves are the phase-integral results, whereas the circles were obtained by evaluating the normal-mode solution at 2-Hz increments in the standard manner.

We drew two conclusions from Fig. 9. First, there were significant differences between phase-integral and mode theory for single ducts, and second, the single-duct mode results gave an improved estimate of critical frequency. These results were what prompted us to develop the modified phase-integral approach.

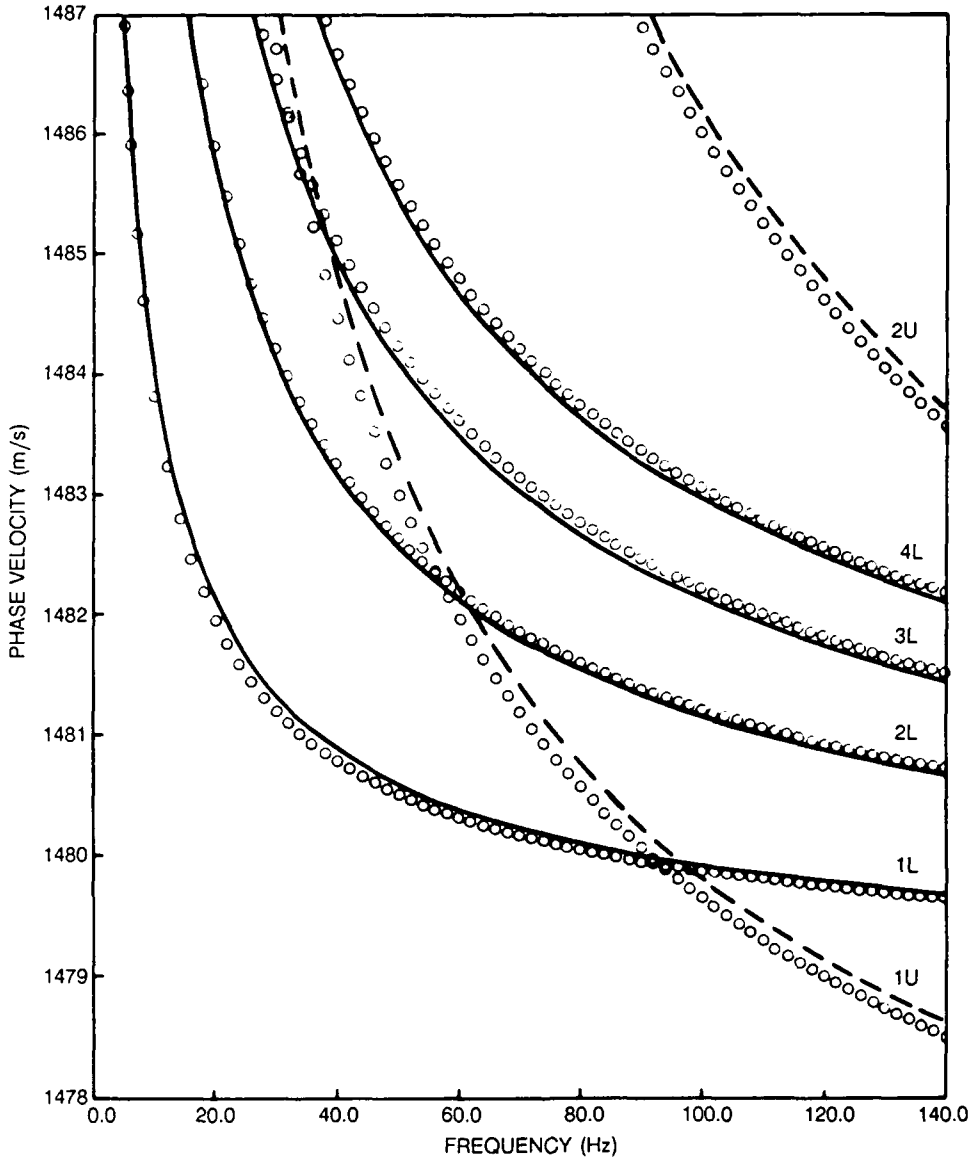

Figure 9. Phase velocity vs frequency for the two single unbounded ducts. The circles are normal-mode evaluations, while the curves are the ray-theory phase-integral results. The curves are identified by mode number and ducts, U for upper and L for lower duct.

We next turn to the modified phase-integral results. The first step is to determine the canonical eigenvalues of Eq. 79 for the two ducts. The value of ρ for the upper and lower duct was 1.684533 and the value for the lower duct was 1.239280. Table 5 presents a summary of the results. Columns 2 and 4 give the roots of Eq. 79 for the upper and lower ducts, respectively. Columns 3 and 5 are the results of Eq. 101 evaluated for these roots.

Table 5. Eignevalues, y, and nonintegral mode number for the two asymmetric unbounded refractive ducts.

Mode Number	Upper Duct		Lower Duct	
	y	Modified n	y	Modified n
1	0.532080	0.976059	0.803585	0.943811
2	1.123907	1.961473	1.806723	1.996193
3	1.600740	2.984143	2.550366	3.009308
4	2.013586	4.004700	3.176687	3.988285

The entire approach was tested by evaluating the phase-integral expressions for the modified values of n. The set of curves was plotted to the scale of Fig. 9. We were most pleased to find that this set of curves passed through the centers of the circles of Fig. 9. The circles of Fig. 9 were determined by a standard normal-mode approach in which the phase velocity is determined by iterating the eigenvalue equation for each frequency and each mode. Thus, a given mode required some 70 sets of iterations to cover the frequency band from 0 to 140 Hz. In contrast, the solution for a given mode of Eq. 81 requires one set of iterations of the canonical eigenvalue equation, and this solution applies to all frequencies, not just those of Fig. 9. Also, the agreement of the modified phase-integral results with the mode solution of Fig. 9 verified not only the modified phase-integral results, but also the normal-mode approach of Eq. 79 and 81, because the modified phase-integral results are based on the solutions of Eq. 79.

We are now in a position to answer a question about Fig. 9 which could not be answered when it was first generated. Observe the larger displacements between ray and mode theory for the upper duct as compared to the lower duct. We initially attributed this to the fact that the ρ for the upper duct was larger than that for the lower duct. However, this conclusion was in error. Consider columns 3 and 5 of Table 5 for mode 1. Here, the n for the upper duct lies closer to 1 than does the n for the lower duct, yet the difference between ray and mode theory is larger for the upper duct. The answer is that $|\gamma_{10}|^{2/3}$, as well as other terms, appears as a factor in dC_p/dn. The $|\gamma_{10}|^{2/3}$ factor is about 7.9 times larger for the upper duct than for the lower duct. This provides the rationale for larger displacements for the upper duct.

There is another way to assess the multiplicative factors of dC_p/dn. The difference between integral and modified n for the upper duct is 0.024. The corresponding difference in phase velocity should be roughly about 2.4% of the difference in phase velocity between mode 2 and mode 1. One may scale the difference between mode 2 and mode 1 in Fig. 9 and verify that this is a fair approximation. Thus, the error in n should not be regarded as absolute but can be scaled by the phase-velocity difference between modes to estimate the effect of the error in n on phase velocity.

We can now address a feature of Fig. 2 and 4, which we passed over in the previous discussion. The reader may have wondered why we were concerned with modified n when the differences between the solid and dashed curves of Fig. 2 and 4 were nil. The answer is that the curves were based on a very small value of $\gamma_1 = 0.02$, with a relatively small displacement between modes. Thus, one should not judge the importance of modified n on Fig. 2 and 4, but rather on Fig. 9, which represents an application to double-duct profiles with much steeper gradients and large displacements between modes.

Figure 10 is the counterpart of Fig. 8, in which the phase-integral results are replaced by the modified phase-integral results. We see that crossing B of the modified phase-integral method provides a much better estimate of the critical frequency than does the estimate of Fig. 8.

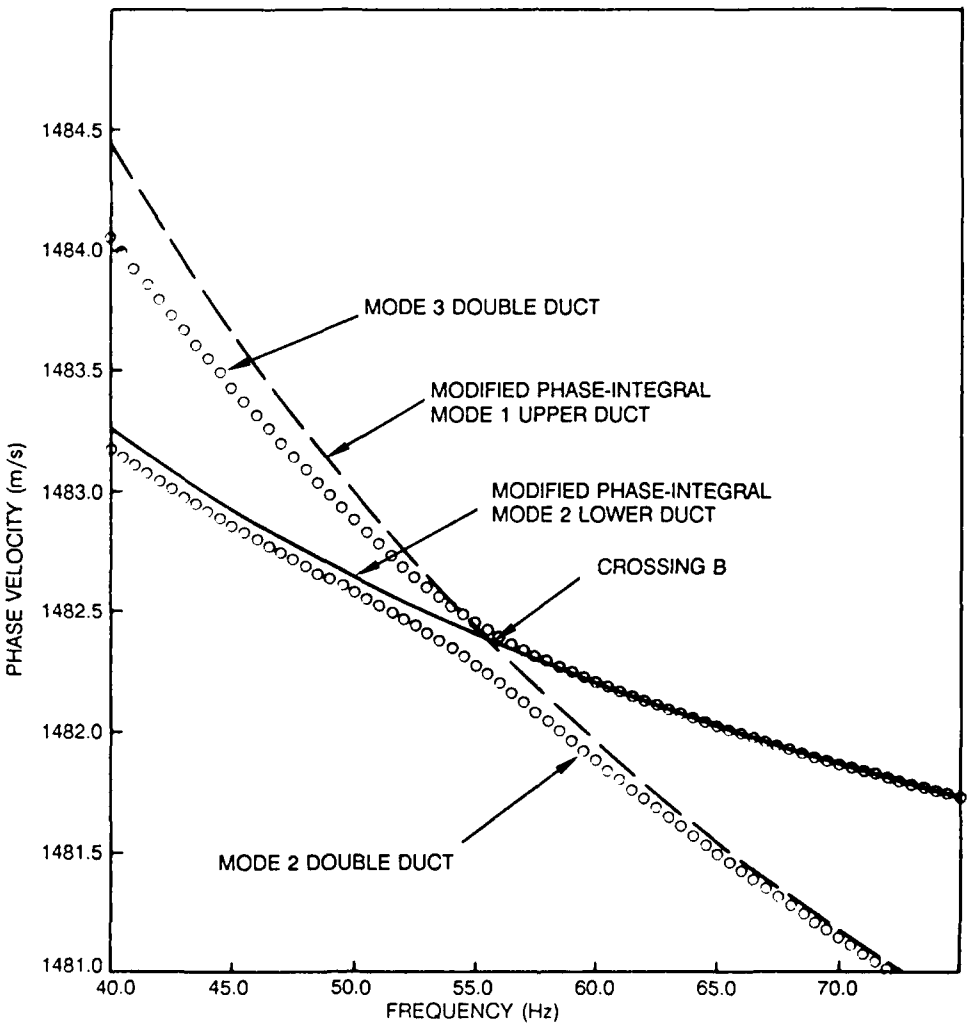

Figure 10. Phase velocity vs frequency for a double duct compared to the modified phase-integral results for the two single ducts.

Figure 11 is the counterpart of Fig. 9 for the group velocity. The circles represent the group velocity as evaluated by conventional mode theory for single ducts. The curves were obtained by evaluating $\tilde{R}/\tilde{T}$ for the phase velocities of Eq. 87. Rather than implement a special normal-mode program, we approximated profile C of Fig. 1 by profile 4 and displaced the surface sound speed so that it was well removed from the axial sound speed. However, at frequencies below about 20 Hz for mode 1 of the upper duct, the effect of the surface begins to show up in Fig. 11 and should be ignored.

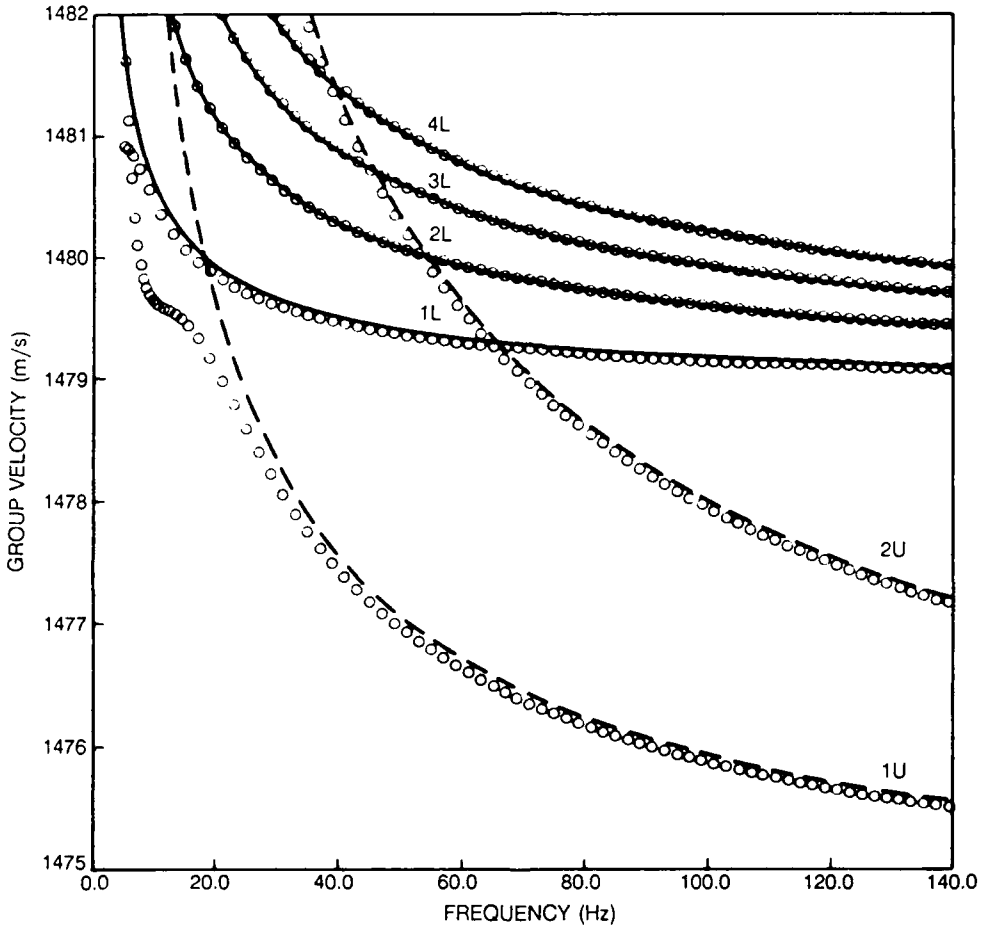

Figure 11. Group velocity vs frequency for the two single unbounded ducts. The circles are normal-mode evaluations, while the curves are obtained from the ray-theory phase-integral results. The curves are identified by mode number and duct, U for upper and L for lower duct.

For the present report we tried two different approaches to duplicating the normal-mode results of Fig. 11. The first approach was to evaluate Eq. 57 at the phase velocities given by Eq. 80 and the roots of Eq. 79. The second approach was to evaluate Eq. 57 at the phase velocities given by Eq. 87 to 89 for the values of n given by Eq. 101. The results of both approaches agreed with each other and were in agreement also with the circles of Fig. 11.

This step provided a numerical verification that the ray-theory results for group velocity are exact whenever the phase-integral results for phase velocity are made exact through the use of nonintegral mode numbers. We will not present the group-velocity results for the double duct as we did for the phase velocity in Fig. 10. The group-velocity behavior near a critical frequency is too involved to deal with here but is presented in Ref. 5.

SECTION 4. CANONICAL EIGENVALUE FORMULATION

Profile 4 of Fig. 1 represents the profile class which first leads to the canonical eigenvalue formulation in two variables. This profile was the logical extension of profile C of Fig. 1, in which the refractive duct is bounded above by a free surface. The boundary condition is given by Eq. 23 and the interface conditions by Eq. 18 and 22, with $i = 1$ and $E_2 = 0$.

The 3 x 3 eigenvalue matrix is expanded and with the use of Eq. 53 and 78 may be written as

$$G(x,y,\rho) = Ai(-x)G_2 - Bi(-x)G_1 = 0 \tag{104}$$

where G_1 is given by Eq. 79 and

$$G_2 = Bi(-y)\,Ai'(-\rho^2 y) + \rho Ai(-\rho^2 y)\,Bi'(-y) \tag{105}$$

We will not present the solution of Eq. 104 here. It is solved by choosing some fixed value of ρ and then iterating to obtain a family of curves of y vs x for the fixed ρ. Each curve corresponds to a mode. We see that Eq. 104 contains two mathematical variables, x and y, and one profile variable, ρ. This can be thought of as an extension to one more mathematical variable as compared to the simpler canonical eigenvalue formulations of Eq. 55, 72, or 79.

Our next step in the formulation is to relate the frequency to the variables. The frequency is not independent of them as it is for the one mathematical variable case. We note that Eq. 54 and 81 hold. If we equate these expressions to eliminate C_p and solve for frequency, we obtain

$$f = (y - x)^{3/2}\,[(C_1/C_2)^2 - 1]^{-3/2}\,|\gamma_1|\pi^{-1} \tag{106}$$

The first factor in Eq. 106 can be evaluated as a function of x by using the solutions of the canonical eigenvalue equation. We refer to a plot of $(y - x)^{3/2}$ vs x as a canonical frequency plot. From this plot, the frequency may be obtained by a simple scale factor obtained by evaluating the remaining factors of Eq. 106 for the specific desired profile parameters. Once the frequency has been evaluated from Eq. 106, Eq. 54 may be used to determine the phase velocity as a function of frequency.

Reference 6 extends the method to any piecewise continuous profile of the form of Eq. 1. The arguments of the Airy functions in the eigenvalue equation can be written as linear combinations of x and y with coefficients that are independent of f, C_p, C_1, C_2,

and γ_1 and depend on the remaining profile parameters. Canonical eigenvalue solutions have been generated for one and two-layer bounded profiles. Reference 7 presents results for the one-layer bounded profiles.

Although the canonical eigenvalue approach can be applied to profiles in which the deepest layer is unbounded, as, for example, profile 4 of Fig. 1, there is a problem which does not arise for bounded profiles. The canonical eigenvalue approach gives two sets of solutions. The first set applies for $C_1 > C_2$, as illustrated by profile 4 of Fig. 1. The second set applies for $C_1 < C_2$, as illustrated by the mirror image of profile 4. The problem is that the second set of solutions is spurious and incorrect. The reason is that the eigenvalue formulation is predicated on Ai as the solution in the unbounded layer with positive slope. However, the second set of solutions corresponds to an unbounded layer with negative slope, which involves the modified Hankel function h_2 as considered in the discussions of Eq. 27. Thus, in the case of an unbounded profile, one must treat one eigenvalue equation for $C_1 > C_2$ and a second eigenvalue equation for $C_1 < C_2$. In the case of bounded profiles, one eigenvalue equation suffices for both conditions. This complication is the reason for deferring the presentation of the solution for unbounded profiles until after the solution for bounded profiles has been presented.

Profile 4 is useful in illustrating why we provided in Section 1 a full-blown ray-theory treatment of the phase integral method. Here, as with most sound-speed profiles, one cannot solve the phase-integral equation for phase velocity in closed form. Equations 42 and 43 provide for the iterative solution. Indeed, the formulation of Eq. 34 allows one to evaluate the phase velocity for any sound-speed profile, provided that one has the ray-theory solutions for $\tilde{T}$ and $\tilde{R}$.

There is a fundamental problem in the standard ray-theory approach to profile 4. This is a $\pi/2$ jump in phase for rays which just reflect from the surface as compared to those which form a refractive apex just below the surface. The modified ray theory of Ref. 16 solves this problem. In this treatment, $\tilde{R}$ and $\tilde{T}$ are functions of f, and the phase shift associated with the surface is a continuous function of phase velocity. Section 1 provides the fundamental background for an article in preparation which incorporates the modified ray theory of Ref. 16 into the phase-integral method and compares these solutions with those of mode theory.

We are now in a position to explain our interest in nonintegral mode numbers. The use of nonintegral mode numbers represents an empirical process which has no interpretation in terms of wave theory. Moreover, the curves of Fig. 10 could have been generated directly from the canonical eigenvalues, without any use of nonintegral mode numbers. The only advantage in Fig. 10 to nonintegral mode numbers is that we could use the same computer routines as used in Fig. 8 to generate the phase-integral results for integral values of n. The advantage of nonintegral n comes into play for more complicated profiles.

For example, the first step in the phase-integral approach to profile 4 is to determine the nonintegral values of n for the refractive duct with no surface. These values of n are then used in the phase-integral formulation for the duct with surface boundary. At high frequencies, the eigenvalues of profile 4 go to those of the unbounded refractive duct. Thus, the use of nonintegral n guarantees that at high frequencies the phase-integral solution for the phase velocity goes to the exact results of mode theory.

SECTION 5. SUMMARY

This report has reviewed the normal-mode and phase-integral results for three simple ducts. Some of the new results obtained follow:

1. This report presents and compares the normal-mode and phase-integral solutions for the asymmetric refractive duct. The phase-integral solution for the asymmetric refractive duct is shown to be the phase-integral solution for a refractive duct with gradients which are the harmonic mean of the absolute value of those of the asymmetric duct.

2. The phase-velocity solutions of the ray-theory implementation of the phase integral can be brought into complete congruence with the corresponding results of exact normal-mode theory by introducing nonintegral mode numbers in the phase-integral formulation. The use of nonintegral mode numbers is an empirical approach which has no interpretation in terms of wave theory. However, their use will improve the accuracy of the phase-integral method for more complicated ducts, where the high-frequency limit approaches that of one of the simple ducts.

3. Wherever the phase velocities of the phase-integral method and normal-mode theory are congruent, so are the group velocities. When this occurs, the group velocities of both mode and ray theory are given by $\tilde{R}/\tilde{T}$.

4. The results for the asymmetric unbounded refractive ducts are compared with normal-mode results for a double-duct profile with two refractive ducts. The normal-mode result for a single duct was more comparable to the normal-mode result for the double duct than it was to the phase-integral approximation for the single duct.

The concept of canonical eigenvalues has been introduced. In this approach, the eigenvalue equation is written in terms of the dimensionless mathematical variables x and y, where x is the negative of the Airy function argument at the surface (upper interface of layer 1) and y is the negative of the Airy function argument at the bottom of layer 1. The eigenvalue equation may contain other dimensionless parameters which are functions of the sound-speed profile. The positive-gradient half space bounded above by a free surface provides the simplest example. Here, the canonical eigenvalues x are discrete and are given by the zeros of the Airy function $Ai(-x)$. From these canonical eigenvalues, one uses Eq. 54 to generate the customary eigenvalues, C_p as a function of frequency, and the profile parameters C_1 and γ_1. The eigenvalues are referred to as canonical because they apply to an entire class of sound-speed profile rather than to a single profile. The solution for the positive gradient half space bounded above by a rigid surface is similar but with the x given by the zeros of $Ai'(-x)$.

The unbounded refractive duct provides another simple example. Here, the canonical eigenvalue equation contains the variable y as a function of ρ, defined as the cube root of the negative of the ratio of axial gradients. Here, y is solved for the given value of ρ and Eq. 81 is used to generate C_p in terms of frequency and profile parameters. Here, the canonical eigenvalues apply to the class of unbounded refractive profiles with given value of ρ.

The more general case of two mathematical variables is illustrated by the refractive duct bounded above by a rigid surface. Here, the canonical eigenvalues are

not discrete values of x or y but consist of curves of y versus x for a fixed value of ρ. In contrast to the simple ducts previously treated, the frequency is no longer an independent variable. Equation 106 gives the frequency as a function of x and y and the profile parameters C_1, C_2, and γ_1. Either Eq. 54 or 81 may now be used to generate C_p as a function of frequency for the profile parameters and the values of x or y.

The advantages of the canonical method, illustrated in this report, are the application to a class of profiles rather than to a single profile and the reduction by four of the number of parameters in the eigenvalue equation. Other advantages are presented in Ref. 5.

REFERENCES

1. Pedersen, M.A., D.F. Gordon, and D. Edwards, "Evaluation of Propagation for Two Underwater Acoustic Ducts," J. Acoust. Soc. Am. 76S, 38(A) (1984).

2. _____, "Coupling Characteristics Between Two Underwater Acoustic Ducts," Proceedings International Conference on Developments in Marine Acoustics, Sydney, Australia, 37-40, (1984).

3. Gordon, D.F., and M.A. Pedersen, "Frequency Spectrum Characteristics of Underwater Acoustic Propagation in Double Ducts," Extended Abstracts, 12th ICA Associated Symposium in Underwater Acoustics, Halifax, N. S., Canada, 63-64, (1986).

4. _____, "Comparison of Mode and Ray Theory Using Phase and Group Velocity," Proceedings 12th International Congress on Acoustics, Toronto, Canada, Vol. III, H 3-6 (1986).

5. Gordon, D.F., D. Edwards, and M.A. Pedersen, "Frequency Spectrum Characteristics of Underwater Acoustic Propagation in Double Ducts," Naval Ocean Systems Center, San Diego, Calif., NOSC TR 1330 (1990).

6. Pedersen, M.A., D.F. Gordon, and F. Hosmer, "Canonical Eigenvalues, Part I: Naval Ocean Systems Center, San Diego, Calif., NOSC TR 1332 (1990).

7. _____, "Canonical Eigenvalues, Part II: Application to One-Layer Bounded, Underwater-Acoustic Ducts," Naval Ocean Systems Center, San Diego, Calif., NOSC TR 1333. (In process.)

8. Hall, M., D.F. Gordon, and D. White, "Improved Methods of Determining Eigenvalues in Multi-layered Normal-mode Problems," J. Acoust. Soc. Am. 73, 153-162 (1983).

9. Bucker, H.P., "Normal Mode Sound Propagation in Shallow Water," J. Acoust. Soc. Am. 36, 251-258 (1964).

10. Brekhovskikh, L. and Y. Lysanov, *Fundamentals of Ocean Acoustics*, Springer-Verlag Berlin, Heidelberg, New York (1982).

11. Freehafer, J.E., *Propagation of Short Radio Waves*, edited by D.E. Kerr, Dover, New York, pp. 70-87 (1965).

12. Tolstoy, I., and C.S. Clay, *Ocean Acoustics*, McGraw-Hill, New York, 1960.

13. White, D., and D.F. Gordon, "Analysis of Shallow Water Sound Propagation by Normal Mode Theory," J. Acoust. Soc. Am. (A) 34, 605 (1976).

14. Pedersen, M.A., and R.W. McGirr, "Use of Theoretical Controls on Underwater Acoustic Model Evaluation," Naval Ocean Systems Center, San Diego, Calif., TR 758, 130-134 (1982).

15. Pedersen, M.A., D. White, and D.W. Johnson, "Generalized Expansion of Ray Theory in Terms of Phase Velocity," J. Acoust. Soc. Am. 58, 78-96 (1974).

16. Murphy, E.L., and J.A. Davis, "Modified Ray Theory for Bounded Media," J. Acoust. Soc. Am. 56, 1747-1760 (1974).

17. Murphy, E.L., "Modified Ray Theory for the Two-Turning Point Problem," J. Acoust. Soc. Am. 47, 899-908 (1970).

18. Pedersen, M.A., and D.F. Gordon, "Normal-Mode Theory Applied to Short-Range Propagation in an Underwater Acoustic Surface Duct," J. Acoust. Soc. Am. 37, 105-118 (1965).

19. Miller, J.C.P., *The Airy Integral* (Cambridge O. P., Cambridge, England, 1946). British Assoc. for the Advancement of Science, Math tables Pt., Vol. B.

20. Pedersen, M.A., and D.F. Gordon, "Normal-Mode and Ray Theory Applied to Underwater Acoustic Conditions of Extreme Downward Refraction," J. Acoust. Soc. Am. 51, 323-368 (1972).

21. Abramowitz, M., and I.A. Stegun, *Handbook of Mathematical Functions*, National Bureau of Standards Applied Mathematics Series 55, Ninth Printing, pp. 448-449 (1970).

22. Pedersen, M.A., "Theory of the Axial Ray," J. Acoust. Soc. Am. 45, 157-176 (1969).

23. Pedersen, M.A., and D. White, "Ray Theory of the General Epstein Profile", J. Acoust. Soc. Am. 44, 765-786 (1968).

REPORT DOCUMENTATION PAGE

Form Approved
OMB No. 0704-0188

1 AGENCY USE ONLY *(Leave blank)*	2. REPORT DATE	3. REPORT TYPE AND DATES COVERED
	February 1990	Final April 1986 - March 1989

4. TITLE AND SUBTITLE
NORMAL-MODE AND PHASE-INTEGRAL METHODS FOR DETERMINING PHASE AND GROUP VELOCITIES IN SIMPLE UNDERWATER ACOUSTIC DUCTS

5. FUNDING NUMBERS
0601152N
R00N0
712W0901

6. AUTHOR(S)
M. A. Pedersen,
D. F. Gordon, F. Hosmer

7. PERFORMING ORGANIZATION NAME(S) AND ADDRESS(ES)
Naval Ocean Systems Center
San Diego, CA 92152-5000

8. PERFORMING ORGANIZATION REPORT NUMBER
TR 1331

9. SPONSORING/MONITORING AGENCY NAME(S) AND ADDRESS(ES)
Naval Ocean Systems Center
Independent Research, Code 0141

10. SPONSORING/MONITORING AGENCY REPORT NUMBER

11. SUPPLEMENTARY NOTES

12a. DISTRIBUTION/AVAILABILITY STATEMENT
Approved for public release; distribution is unlimited.

12b. DISTRIBUTION CODE

13. ABSTRACT *(Maximum 200 words)*

This theoretical report compares normal-mode and phase-integral results for three simple classes of ducts. These classes are a positive-gradient half space bounded above by a free or a rigid surface and an unbounded refractive duct. The major interest in these simple ducts is that the analysis leads to the concept of canonical eigenvalues. The term "canonical" is used because the eigenvalues apply to an entire class of sound-speed profile rather than to one specific profile as in the customary eigenvalue approach. The general canonical eigenvalue equation contains two dimensionless mathematical variables and a set of dimensionless coefficients that are functions of the profile parameters. The normal-mode and phase-integral results for unbounded refractive ducts are compared with modal results for a double-duct profile with two refractive ducts. Modal results for the two models agree when the double-duct phase velocities of adjacent modes are well separated.

14. SUBJECT TERMS	15. NUMBER OF PAGES
acoustic propagation, group velocities, wave propagation, normal modes	41
	16. PRICE CODE

17. SECURITY CLASSIFICATION OF REPORT	18. SECURITY CLASSIFICATION OF THIS PAGE	19. SECURITY CLASSIFICATION OF ABSTRACT	20. LIMITATION OF ABSTRACT
UNCLASSIFIED	UNCLASSIFIED	UNCLASSIFIED	SAME AS REPORT